Environmental Science & Technology

Article

Cite This: Environ. Sci. Technol. 2019, 53, 14398−14408

Experimental Study of OH-Initiated Heterogeneous Oxidation of Organophosphate Flame Retardants: Kinetics, Mechanism, and Toxicity

Qifan Liu,[†] John Liggio,[*,†] Dongmei Wu,[‡] Amandeep Saini,[†] Sabina Halappanavar,[‡] Jeremy J. B. Wentzell,[†] Tom Harner,[†] Kun Li,[†] Patrick Lee,[†] and Shao-Meng Li[†]

[†]Air Quality Research Division, Environment and Climate Change Canada, Toronto, Ontario M3H 5T4, Canada

[‡]Environmental Health Science and Research Bureau, Health Canada, Ottawa, Ontario K1A 0K9, Canada

Supporting Information

ABSTRACT: The environmental risks and health impacts associated with particulate organophosphate flame retardants (OPFRs), which are ubiquitous in the global atmosphere, have not been adequately assessed due to the lack of data on the reaction kinetics, products, and toxicity associated with their atmospheric transformations. Here, the importance of such transformations for OPFRs are explored by investigating the reaction kinetics, degradation chemical mechanisms, and toxicological evolution of two OPFRs (2-ethylhexyl diphenyl phosphate (EHDP) and diphenyl phosphate (DPhP)) coated on $(NH_4)_2SO_4$ particles upon heterogeneous OH oxidation. The derived reaction rate constants for the heterogeneous loss of EHDP and DPhP are $(1.12 \pm 0.22) \times 10^{-12}$ and $(2.33 \pm 0.14) \times 10^{-12}$ cm^3 $molecules^{-1}$ s^{-1}, respectively. Using recently developed real-time particle chemical composition measurements, particulate products from heterogeneous photooxidation and the associated degradation mechanisms for particulate OPFRs are reported for the first time. Subsequent cytotoxicity analysis of the unreacted and oxidized OPFR particles indicated that the overall particle cytotoxicity was reduced by up to 94% with heterogeneous photooxidation, likely due to a significantly lower cytotoxicity associated with the oxidized OPFR products relative to the parent OPFRs. The present work not only provides guidance for future field sampling for the detection of transformation products of OPFRs, but also strongly supports the ongoing risk assessment of these emerging chemicals and most critically, their products.

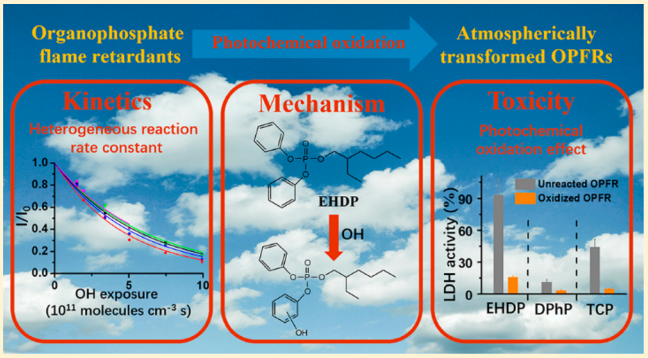

INTRODUCTION

Organophosphate flame retardants (OPFRs) are synthetic chemicals frequently utilized as plasticizers, additives, and antifoaming agents in building materials, electronics, and household products.[1,2] The estimated global market volume of OPFRs is 620 kilotons in 2013 and is expected to increase into the foreseeable future.[3] As OPFRs are not chemically bonded to the materials within commercial products, they are easily emitted into the environment through volatilization, abrasion, and leaching processes.[2] As a result, OPFRs have been frequently detected in various environmental matrices such as surface water,[4] seawater,[5] sediments,[6] snow,[7] soil,[8] household dust,[9] indoor air,[10] and ambient airborne particles[11] over the past decade. Previously measured OPFRs include 2-ethylhexyl diphenyl phosphate (EHDP), diphenyl phosphate (DPhP), tricresyl phosphate (TCP), tris(2-butoxyethyl) phosphate (TBEP), triphenyl phosphate (TPhP), tris(2-ethylhexyl)-phosphate (TEHP), tris-1,3-dichloroisopropyl phosphate (TDCPP), tris-2-chloroethyl phosphate (TCEP), and tris(2-chloroisopropyl) phosphate (TCPP). In the atmosphere, OPFRs have been measured in the global background, in agricultural, urban, rural, and polar regions, with the sum of all measured OPFRs ranging from 69 to 19000 pg m^{-3}.[8,11−16] The ubiquitous presence of OPFRs in the global environment, as well as their potential to induce toxic effects in humans[17−19] have stimulated serious public concerns over their environmental and health risks.[20,21] However, such risks are usually associated with OPFR emissions, with minimal consideration for those associated with the potential secondary atmospheric chemistry.

In the atmosphere, OH radicals are expected to govern the fate of gaseous OPFRs through OH-initiated oxidation reactions, as demonstrated by numerous chemical kinetics studies experimentally[22−24] and modeling.[25−27] However, many atmospheric OPFRs such as EHDP, TCP, TBEP, TPhP, TDCPP, and TCEP are predominantly associated with airborne particles due to their low volatility,[28−30] with chemical fates likely determined by OH-initiated heterogeneous oxidation

Received: September 3, 2019
Revised: October 27, 2019
Accepted: November 22, 2019
Published: November 22, 2019

reactions. During their residence time in the atmosphere, unreacted particulate OPFRs (p-OPFRs) are likely to be gradually transformed to oxidized products through continued photooxidation. The oxidation reactions will form transformation products with the potential to be more toxic than their parent compounds such as the case for polycyclic aromatic hydrocarbons and diesel exhaust.[31,32] Consequently, a complete understanding of the risks associated with many atmospheric p-OPFRs can only be achieved through a comprehensive investigation of the transformation process. This includes knowledge of not only the heterogeneous OH oxidation kinetics, but also the oxidation products, as well as the toxicity profiles of both the parent OPFR and its oxidation products. The incorporation of all of these factors into the risk modeling for these species is of critical importance for an accurate evaluation of their persistence and corresponding health impacts.

Recently, several studies have investigated the heterogeneous OH reactivity of p-OPFRs such as TCP, TBEP, TPhP, and TDCPP.[33−35] However, the heterogeneous oxidation kinetics and thus atmospheric persistence of other commonly used OPFRs such as EHDP and DPhP,[36,37] remain unknown. Furthermore, these previous studies focused only on the heterogeneous OH oxidation kinetics of those species, providing no information on the oxidation products nor the oxidation mechanism. Currently, nontargeted analysis, a promising analytical technique that allows the detection of a broad range of unknown chemicals without specifically targeting individual compounds, is widely used in the detection of pollutants (including OPFRs) in various environmental matrices.[38−40] However, the interpretation of such complex nontargeted data sets is very challenging, as the nature of the identified species (product vs parent molecule) is typically unknown. Given this, it is essential to obtain the transformation product information so that the efficiency of the nontargeted analysis process can be significantly improved through the screening of potential identifiable products in the environmental samples. In addition, the effect of photooxidation (OH oxidation) on the toxicity of p-OPFRs during oxidative aging also remains unclear, despite some limited evidence that exist for aquatic systems (i.e., the toxicity of TCEP in water was significantly reduced upon photooxidation).[41] The potential for causal links between the OH heterogeneous degradation of p-OPFRs, the chemical nature of formed products and the subsequent changes in toxicity, highlights the importance of improved understanding of the interplay between these processes.

In this work, the OH-initiated heterogeneous reactions of EHDP and DPhP coated on $(NH_4)_2SO_4$ particles (used as a proxy for preexisting ambient aerosol) were investigated. Based upon the measured heterogeneous rate constants (k), the degradation lifetimes for these compounds were determined. Concurrently, the particulate OPFR oxidation products were detected using a recently developed extractive electrospray ionization time-of-flight mass spectrometer (EESI-TOFMS),[42,43] capable of determining the heterogeneous oxidation products in real-time, from which a photooxidation mechanism for OPFRs is proposed. In addition, changes in the cytotoxicity of OPFRs as a result of photooxidation were also examined. The results here will further advance the kinetic and mechanistic understanding of the atmospheric transformation for OPFRs, provide new information in support of associated environmental and health risk assessment efforts, and open up a potentially new area of study with advanced instrumentation for the particulate product characterization of existing and future regulated chemicals.

METHODS

Heterogeneous OH Oxidation Experiments. The heterogeneous reactions between OH radicals and OPFRs (EHDP and DPhP) coated onto $(NH_4)_2SO_4$ particles (denoted OPFR@AS) were studied using a photochemical oxidation flow tube reactor described previously[33] and in the Supporting Information (SI; Figure S1). The $(NH_4)_2SO_4$ particles were generated via atomization (TSI, model 3706) of 5.3 mM $(NH_4)_2SO_4$ solution (pH = 6.24), dried through a diffusion drier (TSI, model 3062), and size-selected with a differential mobility analyzer (TSI, model 3081) to obtain a monodispersed $(NH_4)_2SO_4$ particle population with a mode mobility diameter of approximately 95 nm. These dried, monodispersed $(NH_4)_2SO_4$ particles then passed through the headspace of a temperature-controlled Pyrex tube (335−363 K) containing either pure EHDP or DPhP, to generate coated particles with a mode mobility diameter of 125 nm. The coated particles were introduced into a mixing vessel after having passed through an activated carbon denuder to remove volatile organics vapors from the flow.

Upon achieving a steady-state concentration of particulate OPFR (EHDP 10.3 $\mu g\ m^{-3}$; DPhP 12.1 $\mu g\ m^{-3}$) under 254 nm UV light irradiation (Jelight, #82−3309−9) at 298 K in each experiment, O_3 (Ozone Solutions, model TG-10; 0−2 ppm) was introduced into the flow tube reactor. The relative humidity (RH) in the reactor was constantly maintained at 35% by controlling the flow of dry and wet zero air into the reactor. OH radicals were generated by photolysis of O_3 at 254 nm followed by reaction with this water vapor. The O_3 concentration, RH, OPFR concentration, and size distribution of particles exiting the reactor were measured using an O_3 analyzer (2B Technologies, model 202), an RH sensor (Vaisala Inc., model HMP60), an Aerodyne high-resolution time-of-flight aerosol mass spectrometer (HR-TOF-AMS),[44] and a scanning mobility particle sizer (TSI, model 3936), respectively. In offline calibrations, the OH exposure was calculated through the loss of CO due to its reaction with OH,[45] and was in the range of 1.5×10^{11}−2.0×10^{12} molecules cm^{-3} s (see SI). The unreacted and oxidized OPFR@AS particle samples (formed at photochemical ages of 7−9 days; assuming an average atmospheric OH concentration of 1.5×10^6 molecules cm^{-3})[46] were collected on 47 mm Teflon filters (Savillex Inc., #950−450−1192) at the exit of the reactor for subsequent cytotoxicity analysis (see SI). Control experiments demonstrated that O_3 had no effect on the degradation of OPFRs (Figure S2). Further details regarding the chemicals utilized in this study, the flow tube reactor, the OH exposure measurements, and the evaporation of particulate OPFRs are given in the SI. The physicochemical properties of EHDP and DPhP are provided in Table S1.

Detection of Particulate Products. The particulate products of OPFR formed from OH heterogeneous reactions were measured using an EESI-TOFMS previously described[42,43] and in the SI. Unlike the HR-TOF-AMS which utilizes the high energy of electron impact ionization (70 eV; resulting in extreme molecular fragmentation), the EESI-TOFMS uses soft ionization to detect the chemical composition of organic particles in real-time at the molecular level. Briefly, the particle-containing flow exiting the flow tube reactor passed through a multichannel extruded carbon denuder at the inlet of the EESI-TOFMS which removed most of the gaseous species with high efficiency (e.g., >

DOI: 10.1021/acs.est.9b05327
Environ. Sci. Technol. 2019, 53, 14398−14408

Table 1. Summary of Measured and AOPWIN Modeled Rate Constant (k) and Lifetimes (τ) for Seven OPFRs in the Currently Available Literature

	k ($\times 10^{-12}$ cm^3 molecule^{-1} s^{-1})			$\tau_{\_low\ OH}$(days)[a]		$\tau_{\_high\ OH}$(days)[b]	
OPFR	particle phase[c]	aqueous phase[d]	AOPWIN	particle phase	AOPWIN	particle phase	AOPWIN
EHDP	1.12 ± 0.22[e]		39.9	15.9	0.5	6.5	0.2
DPhP	2.33 ± 0.14[e]	20.8 ± 0.33	7.4	7.6	2.4	3.1	1.0
TCP	2.75 ± 0.38[f]	6.30 ± 0.48	13.7	6.5	1.3	2.6	0.5
TBEP	3.06 ± 0.40[f]	13.7 ± 1.03	128.7	5.8	0.1	2.4	0.1
TPhP	2.10 ± 0.19[g]	14.7 ± 0.50	10.8	8.5	1.7	3.4	0.7
TEHP	2.70 ± 0.63[g]		97.9	6.6	0.2	2.7	0.1
TDCPP	0.92 ± 0.09[g]	0.59 ± 0.06	18.1	19.4	1.0	7.9	0.4

[a]Assuming a global mean OH concentration of 6.5 × 10^5 molecules cm^{-3}.[66] [b]Assuming a global mean OH concentration of 1.6 × 10^6 molecules cm^{-3}.[66] [c]Reaction conditions: OPFR coated on $(NH_4)_2SO_4$ particle, 298 K, and 35−38% RH. All values are presented as average k ± standard error (n = 5 experiments). [d]At 298 K, taken from ref 67. [e]This work. [f]Taken from ref 33. [g]Taken from ref 34.

99.6% for pinonic acid).[42] The oxidized OPFR particles then collide with electrospray droplets generated at the end of an electrospray capillary (New Objective; #TT360−50−50−N−5) at a flow rate of 1 μL min^{-1}. Soluble components of the particles were extracted, ionized through a Coulomb explosion of the charged droplets, and detected by a Tofwerk APi-TOFMS. The electrospray working solution was a water−acetonitrile mixture (H_2O−CH_3CN; 1:1 by volume) with 110 ppm of sodium iodide (NaI) as a charge carrier. The potential difference between the ESI probe and APi-TOFMS was set to +2.5 kV. As a result, the mass spectra were recorded in positive ion mode (i.e., Na^+ adducts). For m/z calibration, a series of $[(NaI)_x(CH_3CN)_y(H_2O)_z]Na^+$ (x = 0−3, y = 0−2, z = 0−2) clusters which range from m/z 23 to 491 (Table S2) were utilized.

Sample Preparation for Cytotoxicity Analysis. The unreacted and oxidized particulate OPFR samples collected on the Teflon filters were extracted using an accelerated solvent extractor (Dionex Corporation, ASE 350) with a combination of petroleum ether and acetone solvents (83/17, v/v), followed by reducing the sample to incipient dryness using rotary evaporation and nitrogen blow down, as described previously.[11,12] Dimethyl sulfoxide (DMSO; 1 mL) was then added to reconstitute the volume of the extracted sample for subsequent cytotoxicity analysis.[47] The concentration of OPFR in the DMSO solution is calculated based upon a recovery of 50% for the OPFR collected on the Teflon filter. This analytical method (recovery experiment) was previously validated using spiked/fortified samples, which had been used to measure OPFRs in ambient air samples.[11,12] The recovery of an oxidized OPFR is assumed to be the same as the OPFR precursor since most detected products have similar chemical structures as the OPFR precursor (see below).

Cell Culture and LDH (Lactate Dehydrogenase) Cytotoxicity Assay. Adenocarcinomic human alveolar basal epithelial cells (A549) were maintained as previously described.[47] Briefly, 24 h before exposure, A549 cells (4 × 10^4) were seeded in 96 well plates at a low confluence and incubated in an incubator in a humidified atmosphere of 5% CO_2 with temperature maintained at 335 K. The following day, cells (grown to 90% confluence) were exposed to 7, 14, or 28 mg L^{-1} (n = 3) of unreacted and oxidized OPFR samples. Control cells were exposed to blank filter extracts (n = 3). Cell supernatants were collected at 24 h postexposure for the LDH assay.

A LDH assay kit (Abcam, Toronto, ON, Canada) was used to measure membrane integrity and release of cytoplasmic LDH into the medium.[47] In brief, following the exposure, the 96 well plates were centrifuged at 600 x g for 10 min. The culture supernatants (10 μL) were collected and reacted with 100 μL of LDH Reaction Mix for 30 min at room temperature. The absorbance was measured at 450 nm. The reference wavelength was measured at 650 nm. Changes in the absorbance reflect the degree of cellular permeability, which is indicative of cytotoxicity.

RESULTS AND DISCUSSION

Heterogeneous Oxidation Kinetics. The rate constant of heterogeneous oxidation is quantified by measuring the loss of the particulate OPFR, as estimated by a selected marker ion from the HR-TOF-AMS spectrum.[33] In the current study, the molecular-ion peaks at m/z 362 and m/z 250 were selected as marker ions for EHDP and DPhP, respectively. The changes in the intensities of these two molecular ions as a function of OH exposure from EHDP and DPhP experiments are shown in Figure S3, from which the observed rate constant k_{obs} (cm^3 molecule^{-1} s^{-1}) for the heterogeneous OH oxidation of OPFR can be determined using eq 1:[33,48]

$$\ln \frac{[\mathrm{OPFR}]}{[\mathrm{OPFR}]_0} = \ln \frac{I}{I_0} = -k_{obs}[\mathrm{OH}]t \quad (1)$$

where $[OPFR]_0$, $[OPFR]$, and $[OH]t$ are the initial OPFR concentration (molecules cm^{-3}), the measured OPFR concentration (molecules cm^{-3}) at a given OH exposure, and the OH exposure (molecules cm^{-3} s), respectively. The terms I_0 and I represent the HR-TOF-AMS signal intensities for the selected marker ions (proportional to the OPFR concentration) in the absence and presence of OH radicals. By fitting the data in Figure S3 (I/I_0 vs OH exposure) to an exponential function, k_{obs} can be determined (Table S3). The value of k_{obs} was further corrected for OH gas-phase diffusion using a previously developed empirical formula[49,50] to obtain a true rate constant (k). The values of k for EHDP and DPhP are calculated to be $(1.12 \pm 0.22) \times 10^{-12}$ and $(2.33 \pm 0.14) \times 10^{-12}$ cm^3 molecule^{-1} s^{-1}, respectively (Table 1). The AOPWIN modeled rate constants (estimated based upon the structure−activity relationship method)[51] for EHDP and DPhP are also calculated for comparison as given in Table 1 and would clearly overestimate the k for these two compounds in the particle phase by at least a factor of 3. Such a large deviation between predicted and measured k for these two OPFRs in the particle phase have important implications for their fate in the atmosphere, as discussed below.

DOI: 10.1021/acs.est.9b05327
Environ. Sci. Technol. 2019, 53, 14398−14408

Oxidation Mechanism. As noted above, the molecular ions of most particulate products formed from the heterogeneous OH oxidation of OPFRs cannot be detected with the HR-TOF-AMS due to the high energy of electron impact ionization (Figure S4). However, such molecular level information can be clearly provided by the EESI-TOFMS during an experiment.[42,43] The difference aerosol mass spectra between the oxidized and unreacted EHDP and DPhP (oxidized−unreacted) as measured by the EESI-TOFMS are shown in Figure 1A, and 1B, respectively, from which the oxidation products of these two OPFRs can be identified.

When particulate EHDP was exposed to OH radicals, the signal intensity at m/z 385 which corresponded to $[M+Na^+]$ (M = EHDP molecule) decreased substantially, indicating the degradation of EHDP (Figure 1A). Simultaneously, a series of m/z peaks (ranging from m/z 127 to 433) increased due to the Na^+ adducts with oxidation products, with likely chemical structures for these products given in Table S4. We note that the H_2O−CH_3CN working fluid can also yield clusters of EHDP molecules with H_2O ($[M(H_2O)]Na^+$; m/z 403) and with CH_3CN ($[M(CH_3CN)]Na^+$; m/z 426), with abundances of 2% and 12% of the parent ion ($[M+Na^+]$; m/z 385), respectively. Similarly, for DPhP molecules, the abundances of $[M(H_2O)]Na^+$ (m/z 291) and $[M(CH_3CN)]Na^+$ (m/z 314) clusters are 3% and 9% of the parent ion ($[M+Na^+]$; m/z 273), respectively (Figure 1B). Such findings are consistent with a recent study of α-pinene secondary organic aerosol (SOA) which similarly demonstrated that the abundance of $[M(CH_3CN)]Na^+$ is on the order of 10% of $[M+Na^+]$ (M = SOA components).[42] These results clearly indicate that organic molecules mainly formed $[M+Na^+]$ adducts during the EESI-TOFMS measurements.

Upon the basis of the identified particulate products ($[M+Na^+]$ adducts) from EHDP experiments (Table S4), a chemical mechanism for the heterogeneous OH oxidation of EHDP is proposed in Figure 2 where solid boxes denote molecular formulas that have been detected in these experiments. The reaction channels can be broadly divided into three main categories: OH addition to the phenyl ring (channel 1), OH addition to the phosphate center (channel 2), and OH reactions with the alkyl group (channel 3). In channel 1, products E_1 and E_2 are formed (Figure 2), which are indicative of OH-addition to the phenyl ring and are consistent with the chemical mechanism of OH oxidation of benzene.[52] Channel 2 involves a two-step reaction, i.e., OH addition to the central phosphorus atom, followed by the cleavage of an alkoxy or a phenoxy group from the phosphoric center to generate product E_3 and E_4 (accompanied by the formation of phenol), respectively. Such a transformation pathway has also been reported in the OH oxidation of other OPFRs (TPhP and TCEP) in water.[53−55] Further oxidation of phenol (ring opening reactions) would result in the formation of product a and b (Figure S5), which have been frequently detected in the OH oxidation of aqueous-phase phenol process.[56,57]

In channel 3, oxidation begins with H-abstraction by OH from the alkyl group of EHDP, producing an alkylperoxy radical, which further reacts with HO_2 to yield a hydroperoxide (product E_5). E_5 can then undergo three different reaction pathways. First, E_5 reacts with OH to generate a dihydroperoxide, which then transforms to a carbonyl hydroperoxide (E_6) through the well-established Russell mechanism.[58] The second pathway involves the formation of an alkoxy radical through the photolysis of E_5, which subsequently transforms to a 1,4-hydroxy hydroperoxide (product E_7) via a 1,4-isomerization mechanism. With

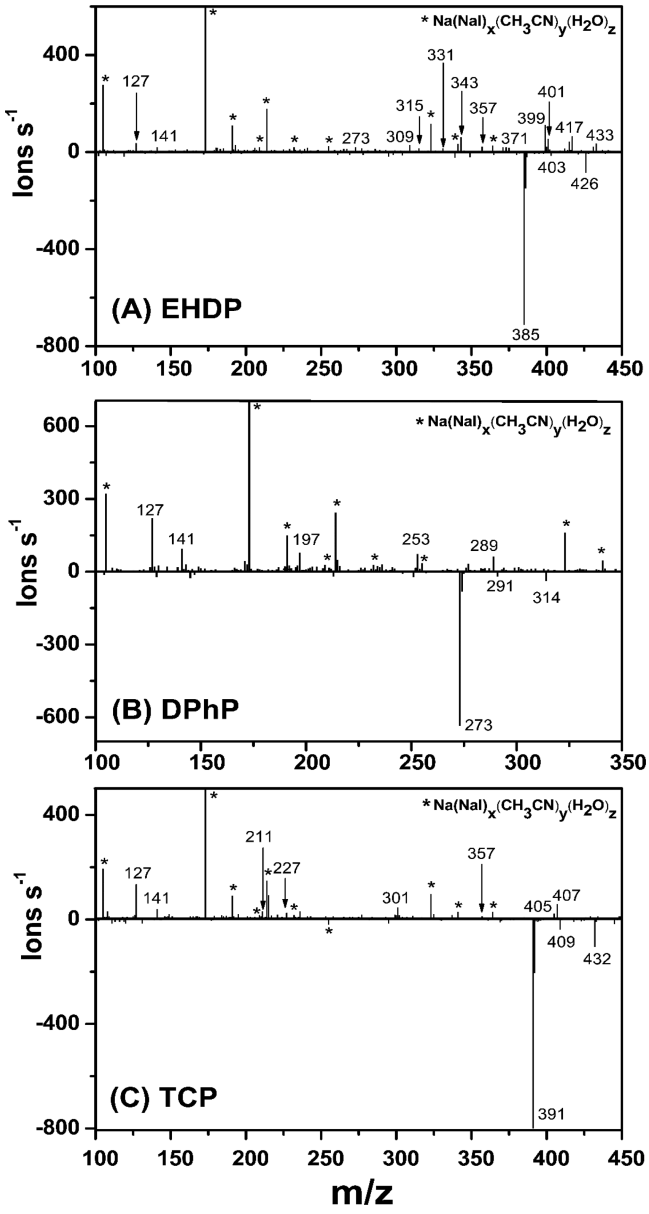

Figure 1. Difference aerosol mass spectra for OPFRs (oxidized−unreacted) as measured by the EESI-TOF-MS: (A) EHDP at an OH exposure of 1.1×10^{12} molecules cm^{-3} s; (B) DPhP at an OH exposure of 7.5×10^{11} molecules cm^{-3} s; (C) TCP at an OH exposure of 7.7×10^{11} molecules cm^{-3} s. Positive and negative values indicate the mass peaks that are enhanced and reduced for OPFRs upon OH exposure, respectively. The $[(NaI)_x(CH_3CN)_y(H_2O)_z]Na^+$ clusters (x = 0−3, y = 0−2, z = 0−2), labeled as (*), are summarized in Table S2. In theory, the intensities of these clusters should be close to zero in the difference aerosol mass spectra, but the difference of two high intensity signals would remain large relative to most ions in the mass spectra.

continued photolysis and isomerization processes, E_7 would be converted to a hydroxy carbonyl (product E_8). In the third pathway, E_5 is converted to a carbonyl (product E_9) according to the above-mentioned Russell mechanism,[58] which can further react with OH to form a carboxylic acid (product E_{10}), and a peracid (product E_{11}). Such a complex mechanism presented above (channel 3) is in good agreement with a previously proposed mechanism for the photooxidation of alkanes.[59,60]

Channel 3 presented here represents a general mechanism for the photooxidation of EHDP as OH can attack various carbon

DOI: 10.1021/acs.est.9b05327
Environ. Sci. Technol. 2019, 53, 14398−14408

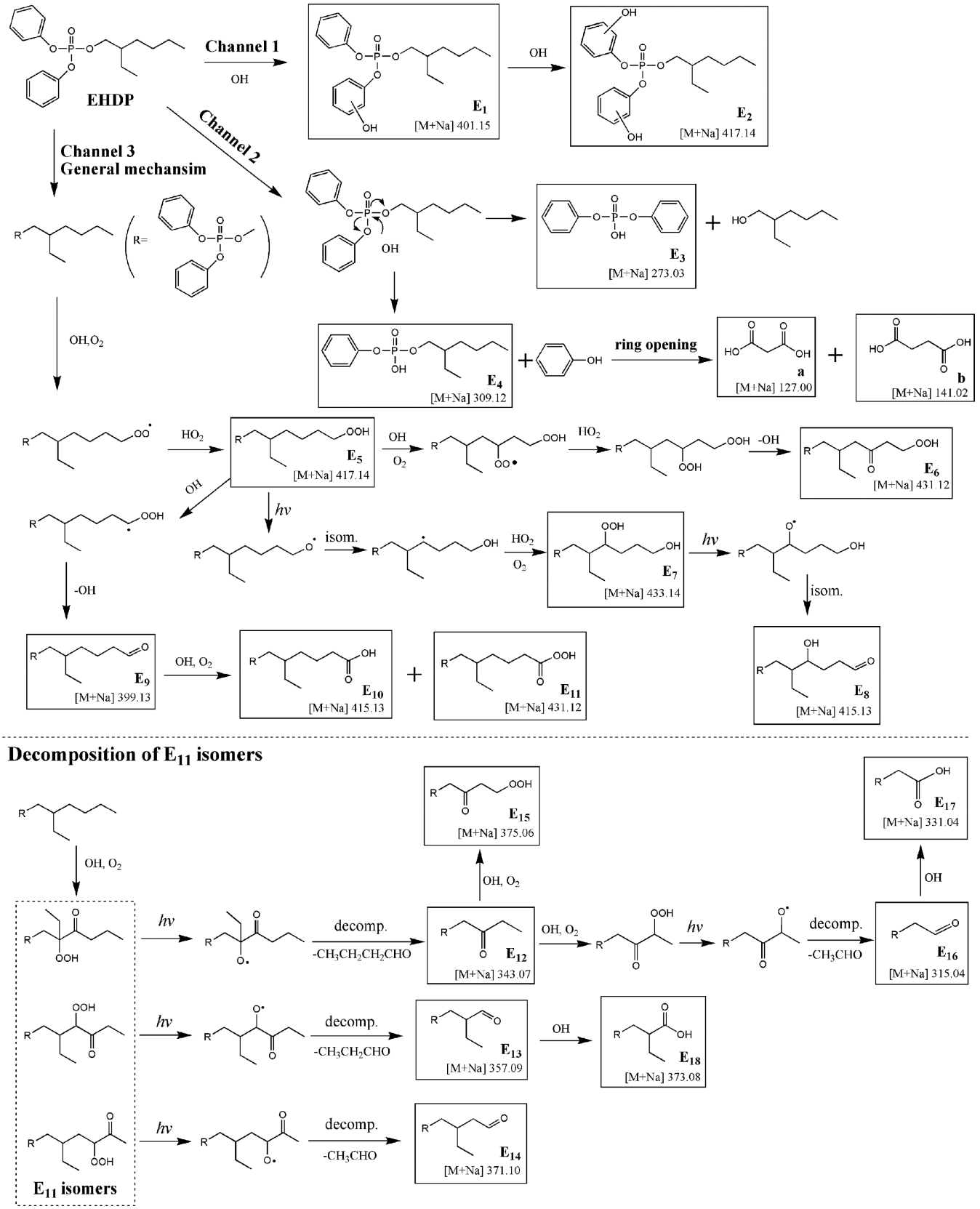

Figure 2. Proposed mechanism for the heterogeneous OH oxidation of particulate EHDP. The particulate products specifically measured by the EESI-TOFMS are indicated in the solid boxes. Note that these identified products could have isomers which are not shown in this figure and EESI-TOFMS is unable to distinguish such isomers from each other.

atoms of the alkyl group, with the potential for other isomers to form. For example, several carbonyl hydroperoxides, which are isomers of E_{11} (see the dashed box in Figure 2), can also be formed through channel 3. Such isomers can undergo photolysis

DOI: 10.1021/acs.est.9b05327
Environ. Sci. Technol. 2019, 53, 14398−14408

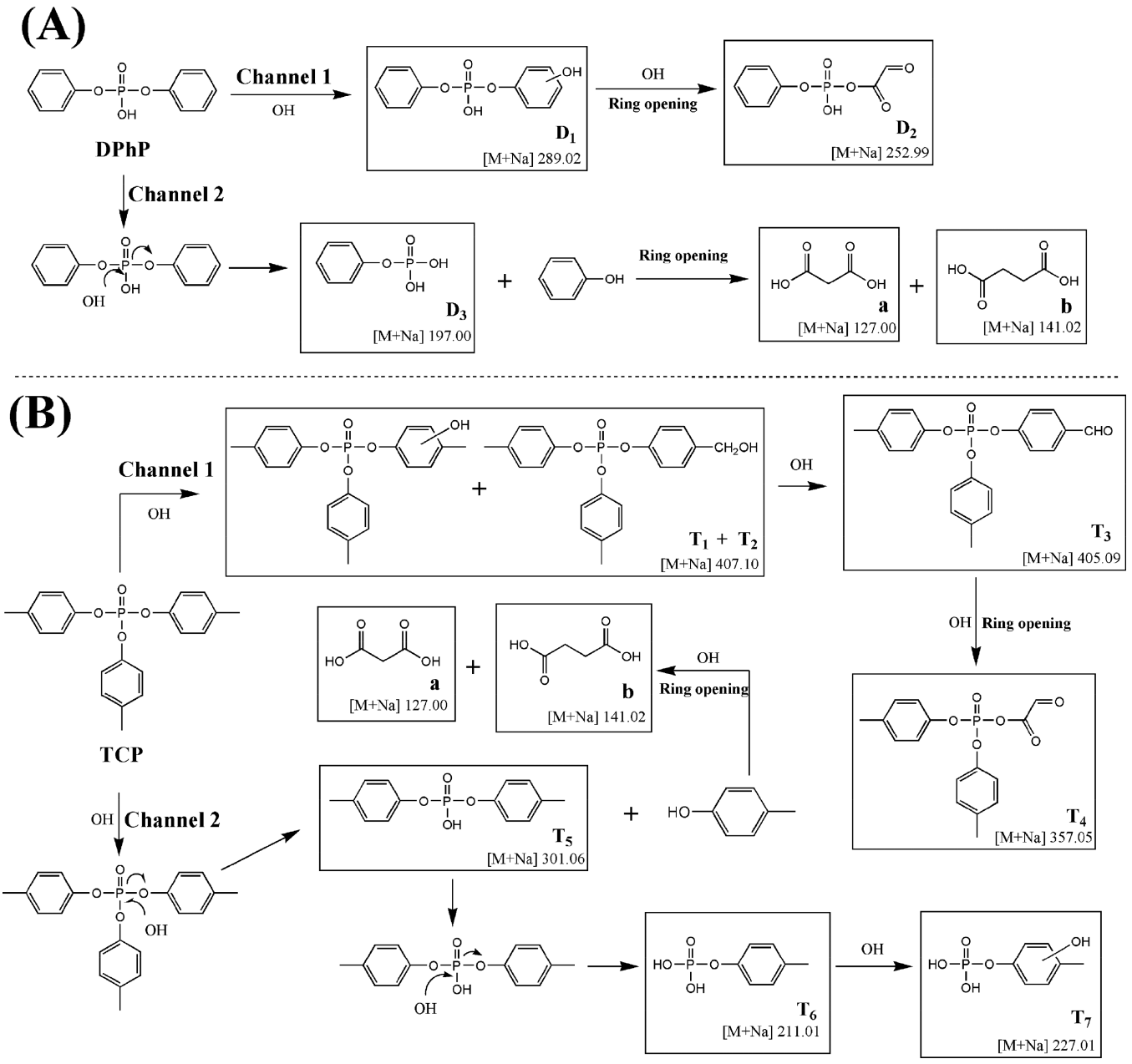

Figure 3. Proposed mechanism for the heterogeneous OH oxidation of (A) particulate DPhP, and (B) particulate TCP. The particulate products specifically measured by the EESI-TOFMS are indicated in the solid box. Note that these identified products could have isomers which are not shown, and EESI-TOFMS is unable to distinguish such isomers from each other.

and decomposition reactions, resulting in the formation of smaller-chain carbonyls (product E_{12}–E_{14}). Further oxidation of these three carbonyls (E_{12}–E_{14}) would lead to the generation of a carbonyl hydroperoxide (product E_{15}), a short-chain carbonyl (product E_{16}), and carboxylic acids (product E_{17} and E_{18}). All these potential products formed from EHDP experiments (product E_1–E_{18}) are summarized in Table S4. Among these products, E_2 and E_5(m/z 417), E_6, E_{11}, and E_{11} isomers in the dashed box (m/z 431), and E_8 and E_{10} (m/z 415) have the same molecular formula, and EESI-TOFMS is unable to distinguish such isomers from each other.

In the case of DPhP, a decrease in the signals of m/z 273, 291, and 314 was observed with OH exposure (Figure 1B). These three peaks correspond to $[M+Na^+]$, $[M(H_2O)]Na^+$, and $[M(CH_3CN)]Na^+$ (M = DPhP molecule), respectively. Concurrently, oxidation of DPhP resulted in the appearance of five mass peaks at m/z 127, 141, 197, 253, and 289 (Figure 1B), corresponding to the Na^+ adducts with product a, b, D_3, D_2, and D_1, respectively (see Figure 3A and Table S5). The possible oxidation mechanism for DPhP is shown in Figure 3A, which follows a similar general mechanistic route as that of EHDP. Briefly, DPhP is observed to react with OH via two different reaction channels, i.e., OH addition to the phenyl ring (channel 1) and OH addition to the phosphate center (channel 2), to form products D_1, D_3, and phenol. Subsequent reactions of OH with D_1 and phenol would produce D_2, a, and b (Figure 3A).

To gain insight into the oxidation mechanism for other OPFRs, the heterogeneous OH oxidation of TCP, an important aryl OPFR,[61] was also investigated (since the heterogeneous oxidation kinetics of TCP has been reported in a previous

DOI: 10.1021/acs.est.9b05327
Environ. Sci. Technol. 2019, 53, 14398−14408

study,[33] the current work only investigated the oxidation mechanism). The difference aerosol mass spectra between the oxidized and unreacted TCP (oxidized−unreacted) as measured by the EESI-TOFMS is shown in Figure 1C, which clearly demonstrated that the signals of m/z at 391, 409, and 432, corresponding to $[M+Na^+]$, $[M(H_2O)]Na^+$, and $[M-(CH_3CN)]Na^+$ (M = TCP molecule), respectively, decreased substantially with OH exposure. Concurrently, a series of m/z peaks which ranged from m/z 127 to 407 increased as shown in Figure 1C and were ascribed to the adducts of Na^+ with oxidation products T_1−T_7, a, and b (Table S6). The chemical transformation mechanism of TCP as shown in Figure 3B is proposed based upon the identified products from Table S6, and is similar to the proposed chemical transformation mechanisms for EHDP and DPhP.

In summary, the three OPFRs investigated in this study undergo similar OH oxidation channels, i.e., OH reacts with the substituent groups of OPFRs (see channel 1 and 3 for EHDP, and channel 1 for DPhP and TCP), and OH addition to the phosphate center (see channel 2 for EHDP, DPhP, and TCP). This suggests that other OPFRs would likely follow similar oxidation channels during OH-initiated heterogeneous oxidation reactions, and thus the products formed through such channels may potentially be predicted.

It should be noted that the HR-TOF-AMS measurement results also provide some limited information with respect to the oxidation products of OPFRs, which are consistent with those measured by the EESI-TOFMS (see SI for additional details). In addition, for a given OPFR, the same EESI-TOFMS m/z peaks were observed at low and high OH exposures (1.5×10^{11} and 1.1×10^{12} molecules cm^{-3} s, respectively), suggesting that the OH reactions would yield similar products over the investigated OH exposure range. However, it is very challenging to quantify these products due to the lack of product standards. Such quantitative analysis may be possible in future studies through a recently developed voltage scanning technique.[62]

It should also be noted that previous studies on gas-phase OPFRs (both experimentally and modeling) are not sufficient to provide comprehensive information on the reaction products and mechanisms for OPFRs.[22,23,25,26] For example, previous experimental studies on gas-phase OPFRs mainly focus on small OPFR molecules (e.g., triethyl phosphate).[22,23] The reported mechanism for these small OPFRs cannot be used to predict the mechanism for large OPFRs (e.g., EHDP) since the mechanism for large OPFRs is expected to be more complex. Also, previous theoretical studies on gas-phase OPFRs (e.g., TPhP) can only predict limited first-generation products, and are unable to predict later-generation products due to the complex secondary chemistry of OPFRs.[25,26] Consequently, these above-mentioned limitations make a direct comparison between the current results (in the particle phase) and previous results (in the gas phase) very difficult. More research is required to investigate the impact of particle phase (vs. gas phase) on the reactivity of OPFRs.

Impact on Cytotoxicity. Extracts of particle samples of unreacted and oxidized OPFR@AS (OPFR coated on $(NH_4)_2SO_4$) were subjected to an in vitro LDH cytotoxicity assay (a measure of cell membrane permeability)[47,63] to assess the impact of photochemical oxidation on the toxicity of these particulate OPFRs. The LDH activity (%) of these particle samples, which is expressed as the percentage increase in the LDH release in A549 cells treated with OPFR@AS extracts relative to the control samples (blank filter extracts), are shown graphically in Figures 4 and S6. Given the relatively non-cytotoxic nature of pure $(NH_4)_2SO_4$ particles (see SI), the

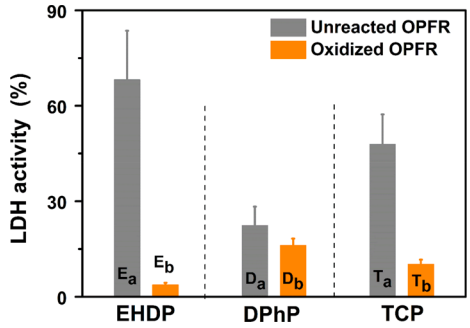

Figure 4. LDH cytotoxicity results from the exposure of A549 cells to unreacted and oxidized EHDP, DPhP, and TCP (at 14 mg L^{-1} dosage). LDH activity (%) is expressed as the percentage increase in the LDH release in A549 cells treated with OPFR extracts relative to the control samples (blank filter extracts). E_a: unreacted EHDP; E_b: oxidized EHDP formed at a photochemical age of 9 days; D_a: unreacted DPhP; D_b: oxidized DPhP formed at a photochemical age of 8 days; T_a: unreacted TCP; and T_b: oxidized TCP formed at a photochemical age of 7 days. The photochemical age is calculated assuming a global mean concentration of 1.5×10^6 molecules cm^{-3} OH.[46]

overall particle cytotoxicity of OPFR@AS (OPFR + $(NH_4)_2SO_4$) is likely caused mainly by the OPFR rather than $(NH_4)_2SO_4$. All of the three pure (unreacted) OPFRs investigated in this study (EHDP, DPhP, and TCP; i.e., sample E_a, D_a, and T_a in Figure 4), produced overt cytotoxicity at 14 mg L^{-1} dosage, as demonstrated by the strong LDH activity of E_a ((68 ± 15)%), D_a ((22 ± 6)%), and T_a ((48 ± 9)%). This is consistent with a previous toxicity study on other OPFRs (TBEP and TCPP) which had similarly shown that exposure to OPFRs at 200 μM dosage (~80 mg L^{-1}) would result in an up to 31% increase in the LDH leakage in A549 cells.[18]

A clear difference between the LDH activity of unreacted and oxidized OFPRs is also observed (Figure 4). As noted in the Methods section and Table S7, EHDP, DPhP, and TCP were oxidized to simulate photochemical ages of 9, 8, and 7 days, respectively. Under such conditions, most OPFR precursors would be transformed to oxidized products due to the OH-initiated degradation process, with an estimated degradation fraction of 73%, 91%, and 92% for EHDP, DPhP, and TCP, respectively (calculated based upon the measured k in Table 1). As a result, the particles was comprised mainly of oxidized products rather than the OPFR precursors. Clearly, the cytotoxic potencies of the three unreacted OPFR@AS particles (E_a, D_a, and T_a) are significantly reduced with increased photochemical oxidation (Figure 4). For example, an estimated photochemical oxidation of 9, 8, and 7 days resulted in a 94%, 28%, and 78% decrease in the LDH activity for EHDP, DPhP, and TCP, respectively (see E_a vs E_b, D_a vs D_b, and T_a vs T_b in Figure 4). These observations have been further verified via a two-way ANOVA analysis with dose and photochemical age as factors (Table S8), which indicate that the results presented above are statistically significant (p-value < 0.05) except for DPhP (likely due to the relatively low LDH activity of DPhP across the investigated dose range; see Figure S6). Nevertheless, the results here suggest that the overall toxicity of oxidized OPFR particles is significantly reduced relative to their corresponding precursors (unreacted OPFR particles). Such an effect is consistent with a recent study, which has similarly

DOI: 10.1021/acs.est.9b05327
Environ. Sci. Technol. 2019, 53, 14398−14408

shown that the toxicity of TCEP in water is significantly reduced upon photooxidation.[41] It should be noted that, while having a lower toxicity, the oxidized OPFR particles (sample E_b, D_b, and T_b in Figure 4) remain able to induce cell membrane damage in A549 cells, as indicated by their low to moderate LDH activities which range from (4 ± 1)% to (16 ± 2)%.

Atmospheric Fate. The atmospheric lifetimes τ ($\tau = 1/k[OH]_{GM}$) of EHDP and DPhP can be determined from the kinetic data obtained in this work (see Table 1 and Figure 5),

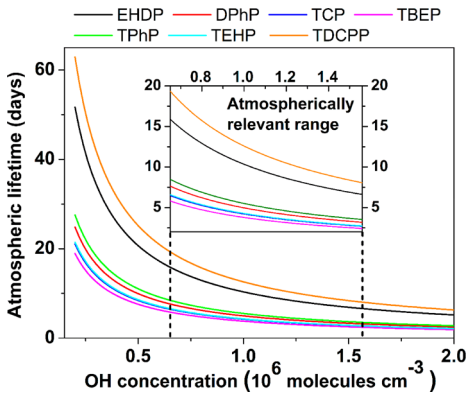

Figure 5. Estimated atmospheric lifetime of seven OPFRs (EHDP, DPhP, TCP, TBEP, TPhP, TEHP, and TDCPP) in the particle phase as a function of OH concentration. These particle lifetimes were calculated based upon the measured k in Table 1. Atmospherically relevant range: global mean OH concentration 6.5×10^5–1.6×10^6 molecules cm^{-3}.[46,65,66]

which are key parameters in the environmental risk assessment for these species.[36,61,64] On the basis of the true reaction rate constant and a global mean OH concentration ($[OH]_{GM}$) which ranges from 6.5×10^5 to 1.6×10^6 molecules cm^{-3} (i.e., an atmospherically relevant range in Figure 5),[46,65,66] the τ_{EHDP} and τ_{DPhP} are estimated to be 6.5–15.9 and 3.1–7.6 days, respectively, depending upon the $[OH]_{GM}$. They are at least three times longer than the estimated τ based upon the AOPWIN derived rate constants (Table 1). This is in agreement with previous results for other particulate OPFRs such as TCP, TBEP, TPhP, TEHP, and TDCPP which also demonstrated an enhanced atmospheric persistence due to significant differences between measured heterogeneous rate constants and those modeled for the gas-phase.[33,34]

The atmospheric lifetimes derived for EHDP and DPhP here can also be placed in context of other OPFRs. As shown in Figure 5, the atmospheric lifetime of DPhP (3.1–7.6 days) is slightly longer than the τ of TBEP (2.4–5.8 days), TCP (2.6–6.5 days), and TEHP (2.7–6.6 days), and is slightly shorter than the τ of TPhP (3.4–8.5 days), but is significantly shorter than the τ of EHDP (6.5–15.9 days) and TDCPP (7.9–19.4 days). The extended lifetime of TDCPP (i.e., lower reactivity) relative to other OPFRs is consistent with its lower reactivity in water relative to other aryl and alkyl phosphates (Table 1).[67] The estimate of atmospheric lifetime for DPhP here suggests that it is sufficiently long to undergo medium-range transport in the atmosphere even though it is less persistent than halogenated OPFRs (TDCPP). However, EHDP is likely to have the potential for long-range atmospheric transport given its longer persistence (up to 15.9 days). This is consistent with a previous field study which found a high concentration of EHDP (up to 298 pg m^{-3}) in ambient particle samples collected in Arctic.[16]

The chemical structures of different OPFRs (EHDP, DPhP, TBEP, TCP, TEHP, TPhP, and TDCPP) were provided in Figure S7.

Implications. The current work, while providing new heterogeneous kinetic data for several species, also presents detailed information on the photooxidation mechanism and cytotoxicity profiles for particulate OPFRs present in atmosphere. Given that no other oxidation product and toxicity information is presently available with respect to atmospherically transformed particulate OPFRs, the present work not only sheds light on field study data for OPFRs, but also strongly supports the ongoing risk assessment of these emerging chemicals. For example, the identified oxidation products from the current laboratory experiments can be used to guide future field measurements for OPFRs by screening for these products in samples collected from ambient air in conjunction with nontargeted analysis. In addition, on the basis of the methods utilized in this work which provide product characterization, the potential may also exist to ultimately rank the chemical products formed in terms of toxicity, and may be expanded to include the products from a variety of OPFRs and other chemicals of emerging concern. In doing so, the risk assessment for precursors and oxidation products can be more effectively prioritized.

Considering that the toxicities of the OPFR-containing particles investigated here (EHDP, DPhP, and TCP) are reduced upon photochemical oxidation (see above), it is possible that the toxicities of other OPFRs will be similarly reduced upon atmospheric exposure, thus reducing the overall risks associated with the OPFRs released into the atmosphere. However, as only one cytotoxicity assay (LDH release) and one cell type (A549 cell) were utilized in the current work, the observed toxicity reduction here may not be the case for other OPFRs using different toxicity assays and different cell types. Further study is warranted to assess the impact of photooxidation on the toxicity of other types of OPFRs (e.g., halogenated OPFRs) and using different toxicity assays (e.g., in vivo and in vitro ATP and resazurin reduction assays) and different cells (e.g., J774 cell). In addition, in the real atmosphere, the heterogeneous oxidation of particulate OPFRs is likely to be more complicated than the present laboratory results indicate, given the complex mixing state of ambient particles (i.e., the effect of other organic coatings) which has been demonstrated to reduce OH reaction kinetics.[34] Further experimental study is hence necessary to better understand the impact of mixing state on the overall toxicity of OPFR-containing particles. While further research is needed, the experimental approach and observations outlined here open up a new research avenue for the persistent organic pollutants (POPs) research community to more deeply investigate the complexity of the atmospheric transformations of POPs and other chemicals and associated toxicity.

■ ASSOCIATED CONTENT

Supporting Information

The Supporting Information is available free of charge at https://pubs.acs.org/doi/10.1021/acs.est.9b05327.

Details of the flow tube reactor and EESI-TOFMS and other experimental details; HR-TOF-AMS measurement results; LDH cytotoxicity results of unreacted OPFRs, oxidized OPFRs, and $(NH_4)_2SO_4$ particles; and comparison of AOPWIN predicted gas-phase k and measured

DOI: 10.1021/acs.est.9b05327
Environ. Sci. Technol. 2019, 53, 14398−14408

particle-phase and aqueous-phase k for several OPFRs (PDF)

AUTHOR INFORMATION

Corresponding Author

*Phone: 1-416-739-4840; e-mail: John.Liggio@canada.ca.

ORCID

Qifan Liu: 0000-0003-0033-5313
John Liggio: 0000-0003-3683-4595
Amandeep Saini: 0000-0003-0880-1147
Tom Harner: 0000-0001-9026-3645
Kun Li: 0000-0003-2970-037X

Notes

The authors declare no competing financial interest.

ACKNOWLEDGMENTS

This research was partly funded by the Chemicals Management Plan (CMP) of Canada.

REFERENCES

(1) Wei, G. L.; Li, D. Q.; Zhuo, M. N.; Liao, Y. S.; Xie, Z. Y.; Guo, T. L.; Li, J. J.; Zhang, S. Y.; Liang, Z. Q. Organophosphorus flame retardants and plasticizers: sources, occurrence, toxicity and human exposure. *Environ. Pollut.* **2015**, *196*, 29−46.

(2) Van der Veen, I.; de Boer, J. Phosphorus flame retardants: properties, production, environmental occurrence, toxicity and analysis. *Chemosphere* **2012**, *88* (10), 1119−1153.

(3) China Market Research Reports. *Global and China Flame Retardant Industry Report*; http://www.chinamarketresearchreports.com/114859.html, 2014−2016.

(4) Kim, U. J.; Kannan, K. Occurrence and distribution of organophosphate flame retardants/plasticizers in surface waters, tap water, and rainwater: implications for human exposure. *Environ. Sci. Technol.* **2018**, *52* (10), 5625−5633.

(5) Li, J.; Xie, Z.; Mi, W.; Lai, S.; Tian, C.; Emeis, K. C.; Ebinghaus, R. Organophosphate esters in air, snow, and seawater in the North Atlantic and the Arctic. *Environ. Sci. Technol.* **2017**, *51* (12), 6887−6896.

(6) Cristale, J.; Vázquez, A. G.; Barata, C.; Lacorte, S. Priority and emerging flame retardants in rivers: occurrence in water and sediment, Daphnia magna toxicity and risk assessment. *Environ. Int.* **2013**, *59*, 232−243.

(7) Marklund, A.; Andersson, B.; Haglund, P. Traffic as a source of organophosphorus flame retardants and plasticizers in snow. *Environ. Sci. Technol.* **2005**, *39* (10), 3555−3562.

(8) Kurt-Karakus, P.; Alegria, H.; Birgul, A.; Gungormus, E.; Jantunen, L. Organophosphate ester (OPEs) flame retardants and plasticizers in air and soil from a highly industrialized city in Turkey. *Sci. Total Environ.* **2018**, *625*, 555−565.

(9) Tan, H.; Yang, L.; Yu, Y.; Guan, Q.; Liu, X.; Li, L.; Chen, D. Co-Existence of organophosphate di-and tri-esters in house dust from south china and midwestern united states: implications for human exposure. *Environ. Sci. Technol.* **2019**, *53* (9), 4784−4793.

(10) Yang, C.; Harris, S. A.; Jantunen, L. M.; Siddique, S.; Kubwabo, C.; Tsirlin, D.; Latifovic, L.; Fraser, B.; St-Jean, M.; De La Campa, R.; You, H.; Kulka, R.; Diamond, M. L. Are cell phones an indicator of personal exposure to organophosphate flame retardants and plasticizers? *Environ. Int.* **2019**, *122*, 104−116.

(11) Rauert, C.; Schuster, J. K.; Eng, A.; Harner, T. Global atmospheric concentrations of brominated and chlorinated flame retardants and organophosphate esters. *Environ. Sci. Technol.* **2018**, *52* (5), 2777−2789.

(12) Saini, A.; Clarke, J.; Jariyasopit, N.; Rauert, C.; Schuster, J. K.; Halappanavar, S.; Evans, G. J.; Su, Y.; Harner, T. Flame retardants in urban air: a case study in Toronto targeting distinct source sectors. *Environ. Pollut.* **2019**, *247*, 89−97.

(13) Salamova, A.; Ma, Y.; Venier, M.; Hites, R. A. High levels of organophosphate flame retardants in the Great Lakes atmosphere. *Environ. Sci. Technol. Lett.* **2014**, *1* (1), 8−14.

(14) Möller, A.; Sturm, R.; Xie, Z.; Cai, M.; He, J.; Ebinghaus, R. Organophosphorus flame retardants and plasticizers in airborne particles over the Northern Pacific and Indian Ocean toward the polar regions: evidence for global occurrence. *Environ. Sci. Technol.* **2012**, *46* (6), 3127−3134.

(15) Sühring, R.; Diamond, M. L.; Scheringer, M.; Wong, F.; Pućko, M.; Stern, G.; Burt, A.; Hung, H.; Fellin, P.; Li, H.; Jantunen, L. M. Organophosphate esters in Canadian Arctic air: occurrence, levels and trends. *Environ. Sci. Technol.* **2016**, *50* (14), 7409−7415.

(16) Salamova, A.; Hermanson, M. H.; Hites, R. A. Organophosphate and halogenated flame retardants in atmospheric particles from a European Arctic site. *Environ. Sci. Technol.* **2014**, *48* (11), 6133−6140.

(17) Xiang, P.; Liu, R. Y.; Li, C.; Gao, P.; Cui, X. Y.; Ma, L. Q. Effects of organophosphorus flame retardant TDCPP on normal human corneal epithelial cells: implications for human health. *Environ. Pollut.* **2017**, *230*, 22−30.

(18) An, J.; Hu, J.; Shang, Y.; Zhong, Y.; Zhang, X.; Yu, Z. The cytotoxicity of organophosphate flame retardants on HepG2, A549 and Caco-2 cells. *J. Environ. Sci. Health, Part A: Toxic/Hazard. Subst. Environ. Eng.* **2016**, *51* (11), 980−988.

(19) Zhang, Q.; Ji, C.; Yin, X.; Yan, L.; Lu, M.; Zhao, M. Thyroid hormone-disrupting activity and ecological risk assessment of phosphorus-containing flame retardants by in vitro, in vivo and in silico approaches. *Environ. Pollut.* **2016**, *210*, 27−33.

(20) DiGangi, J. A public interest guide to toxic flame retardant chemicals. *International POPs Elimination Network*; https://ipen.org/pdfs/ipen_flame_retardants_2012_06.pdf, 2012.

(21) Cordner, A.; Brown, P. A multisector alliance approach to environmental social movements: flame retardants and chemical reform in the United States. *Environmental Sociology* **2015**, *1* (1), 69−79.

(22) Aschmann, S. M.; Long, W. D.; Atkinson, R. Temperature-dependent rate constants for the gas-phase reactions of OH radicals with 1, 3, 5-trimethylbenzene, triethyl phosphate, and a series of alkylphosphonates. *J. Phys. Chem. A* **2006**, *110* (23), 7393−7400.

(23) Aschmann, S. M.; Tuazon, E. C.; Atkinson, R. Atmospheric chemistry of diethyl methylphosphonate, diethyl ethylphosphonate, and triethyl phosphate. *J. Phys. Chem. A* **2005**, *109* (10), 2282−2291.

(24) Laversin, H.; El Masri, A.; Al Rashidi, M.; Roth, E.; Chakir, A. Kinetic of the gas-phase reactions of OH radicals and Cl atoms with diethyl ethylphosphonate and triethyl phosphate. *Atmos. Environ.* **2016**, *126*, 250−257.

(25) Yu, Q.; Xie, H. B.; Chen, J. Atmospheric chemical reactions of alternatives of polybrominated diphenyl ethers initiated by OH: A case study on triphenyl phosphate. *Sci. Total Environ.* **2016**, *571*, 1105−1114.

(26) Li, C.; Zheng, S.; Chen, J.; Xie, H. B.; Zhang, Y. N.; Zhao, Y.; Du, Z. Kinetics and mechanism of OH-initiated atmospheric oxidation of organophosphorus plasticizers: A computational study on tri-p-cresyl phosphate. *Chemosphere* **2018**, *201*, 557−563.

(27) Li, C.; Chen, J.; Xie, H. B.; Zhao, Y.; Xia, D.; Xu, T.; Li, X.; Qiao, X. Effects of atmospheric water on· OH-initiated oxidation of organophosphate flame retardants: a DFT investigation on TCPP. *Environ. Sci. Technol.* **2017**, *51* (9), 5043−5051.

(28) Möller, A.; Xie, Z.; Caba, A.; Sturm, R.; Ebinghaus, R. Organophosphorus flame retardants and plasticizers in the atmosphere of the North Sea. *Environ. Pollut.* **2011**, *159* (12), 3660−3665.

(29) Carlsson, H.; Nilsson, U.; Becker, G.; Östman, C. Organophosphate ester flame retardants and plasticizers in the indoor environment: analytical methodology and occurrence. *Environ. Sci. Technol.* **1997**, *31* (10), 2931−2936.

(30) Sühring, R.; Wolschke, H.; Diamond, M. L.; Jantunen, L. M.; Scheringer, M. Distribution of organophosphate esters between the gas and particle phase−model predictions vs measured data. *Environ. Sci. Technol.* **2016**, *50* (13), 6644−6651.

DOI: 10.1021/acs.est.9b05327
Environ. Sci. Technol. 2019, 53, 14398−14408

(31) Antiñolo, M.; Willis, M. D.; Zhou, S.; Abbatt, J. P. Connecting the oxidation of soot to its redox cycling abilities. *Nat. Commun.* **2015**, *6*, 6812.
(32) Li, Q.; Wyatt, A.; Kamens, R. M. Oxidant generation and toxicity enhancement of aged-diesel exhaust. *Atmos. Environ.* **2009**, *43* (5), 1037−1042.
(33) Liu, Q.; Liggio, J.; Li, K.; Lee, P.; Li, S. M. Understanding the impact of relative humidity and coexisting soluble iron on the OH-initiated heterogeneous oxidation of organophosphate flame retardants. *Environ. Sci. Technol.* **2019**, *53* (12), 6794−6803.
(34) Liu, Y.; Liggio, J.; Harner, T.; Jantunen, L.; Shoeib, M.; Li, S. M. Heterogeneous OH initiated oxidation: a possible explanation for the persistence of organophosphate flame retardants in air. *Environ. Sci. Technol.* **2014**, *48* (2), 1041−1048.
(35) Liu, Y.; Huang, L.; Li, S. M.; Harner, T.; Liggio, J. OH-initiated heterogeneous oxidation of tris-2-butoxyethyl phosphate: implications for its fate in the atmosphere. *Atmos. Chem. Phys.* **2014**, *14* (22), 12195−12207.
(36) Brooke, D. N.; Crookes, M. J.; Quarterman, P.; Burns, J. *Environmental Risk Evaluation Report: 2-Ethylhexyl Diphenyl Phosphate (CAS no. 1241−94−7)*; https://assets.publishing.service.gov.uk/government/uploads/system/uploads/attachment_data/file/290842/scho0809bqty-e-e.pdf, 2009.
(37) Björnsdotter, M. K.; Romera-García, E.; Borrull, J.; de Boer, J.; Rubio, S.; Ballesteros-Gómez, A. Presence of diphenyl phosphate and aryl-phosphate flame retardants in indoor dust from different microenvironments in Spain and the Netherlands and estimation of human exposure. *Environ. Int.* **2018**, *112*, 59−67.
(38) Giorio, C.; Bortolini, C.; Kourtchev, I.; Tapparo, A.; Bogialli, S.; Kalberer, M. Direct target and non-target analysis of urban aerosol sample extracts using atmospheric pressure photoionisation high-resolution mass spectrometry. *Chemosphere* **2019**, *224*, 786−795.
(39) Ouyang, X.; Weiss, J. M.; de Boer, J.; Lamoree, M. H.; Leonards, P. E. Non-target analysis of household dust and laundry dryer lint using comprehensive two-dimensional liquid chromatography coupled with time-of-flight mass spectrometry. *Chemosphere* **2017**, *166*, 431−437.
(40) Tousova, Z.; Froment, J.; Oswald, P.; Slobodník, J.; Hilscherova, K.; Thomas, K. V.; Tollefsen, K. E.; Reid, M.; Langford, K.; Blaha, L. Identification of algal growth inhibitors in treated waste water using effect-directed analysis based on non-target screening techniques. *J. Hazard. Mater.* **2018**, *358*, 494−502.
(41) Liu, J.; Ye, J.; Chen, Y.; Li, C.; Ou, H. UV-driven hydroxyl radical oxidation of tris (2-chloroethyl) phosphate: Intermediate products and residual toxicity. *Chemosphere* **2018**, *190*, 225−233.
(42) Lopez-Hilfiker, F. D.; Pospisilova, V.; Huang, W.; Kalberer, M.; Mohr, C.; Stefenelli, G.; Thornton, J. A.; Baltensperger, U.; Prévôt, A. S. H.; Slowik, J. G. An extractive electrospray ionization time-of-flight mass spectrometer (EESI-TOF) for online measurement of atmospheric aerosol particles. *Atmos. Meas. Tech.* **2019**, *12*, 4867−4886.
(43) Qi, L.; Chen, M.; Stefenelli, G.; Pospisilova, V.; Tong, Y.; Bertrand, A.; Hueglin, C.; Ge, X.; Baltensperger, U.; Prévôt, A. S. H.; Slowik, J. G. Organic aerosol source apportionment in Zurich using an extractive electrospray ionization time-of-flight mass spectrometer (EESI-TOF-MS)-Part 2: biomass burning influences in winter. *Atmos. Chem. Phys.* **2019**, *19*, 8037−8062.
(44) DeCarlo, P. F.; Kimmel, J. R.; Trimborn, A.; Northway, M. J.; Jayne, J. T.; Aiken, A. C.; Gonin, M.; Fuhrer, K.; Horvath, T.; Docherty, K. S.; Worsnop, D. R.; Jimenez, J. L. Field-deployable, high-resolution, time-of-flight aerosol mass spectrometer. *Anal. Chem.* **2006**, *78* (24), 8281−8289.
(45) Liu, Y.; Sander, S. P. Rate constant for the OH + CO reaction at low temperatures. *J. Phys. Chem. A* **2015**, *119* (39), 10060−10066.
(46) Mao, J.; Ren, X.; Brune, W. H.; Olson, J. R.; Crawford, J. H.; Fried, A.; Huey, L. G.; Cohen, R. C.; Heikes, B.; Singh, H. B.; Blake, D. R.; Sachse, G. W.; Diskin, G. S.; Hall, S. R.; Shetter, R. E. Airborne measurement of OH reactivity during INTEX-B. *Atmos. Chem. Phys.* **2009**, *9* (1), 163−173.
(47) Jariyasopit, N.; Harner, T.; Wu, D.; Williams, A.; Halappanavar, S.; Su, K. Mapping indicators of toxicity for polycyclic aromatic compounds in the atmosphere of the Athabasca oil sands region. *Environ. Sci. Technol.* **2016**, *50* (20), 11282−11291.
(48) Chan, M. N.; Zhang, H.; Goldstein, A. H.; Wilson, K. R. Role of water and phase in the heterogeneous oxidation of solid and aqueous succinic acid aerosol by hydroxyl radicals. *J. Phys. Chem. C* **2014**, *118* (50), 28978−28992.
(49) Fuks, N. A.; Sutugin, A. G. *Highly Dispersed Aerosols*; Butterworth-Heinemann: Newton, MA, 1970.
(50) Worsnop, D.; Morris, J.; Shi, Q.; Davidovits, P.; Kolb, C. A chemical kinetic model for reactive transformations of aerosol particles. *Geophys. Res. Lett.* **2002**, *29* (20), 57-1.
(51) *Atmospheric Oxidation Program for Microsoft Windows (AOPWIN)*; U.S. Environmental Protection Agency, 2000.
(52) Volkamer, R.; Klotz, B.; Barnes, I.; Imamura, T.; Wirtz, K.; Washida, N.; Becker, K. H.; Platt, U. OH-initiated oxidation of benzene Part I. Phenol formation under atmospheric conditions. *Phys. Chem. Chem. Phys.* **2002**, *4* (9), 1598−1610.
(53) Song, Q.; Feng, Y.; Liu, G.; Lv, W. Degradation of the flame retardant triphenyl phosphate by ferrous ion-activated hydrogen peroxide and persulfate: Kinetics, pathways, and mechanisms. *Chem. Eng. J.* **2019**, *361*, 929−936.
(54) Du, L.; Wang, X.; Wu, J. Degradation of tri (2-chloroethyl) phosphate by a microwave enhanced heterogeneous Fenton process using iron oxide containing waste. *RSC Adv.* **2018**, *8* (32), 18139−18145.
(55) Wu, L.; Chládková, B.; Lechtenfeld, O. J.; Lian, S.; Schindelka, J.; Herrmann, H.; Richnow, H. H. Characterizing chemical transformation of organophosphorus compounds by 13C and 2H stable isotope analysis. *Sci. Total Environ.* **2018**, *615*, 20−28.
(56) Zhou, L.; Cao, H.; Descorme, C.; Xie, Y. Phenolic compounds removal by wet air oxidation based processes. *Front. Environ. Sci. Eng.* **2018**, *12* (1), 1.
(57) Liotta, L.; Gruttadauria, M.; Di Carlo, G.; Perrini, G.; Librando, V. Heterogeneous catalytic degradation of phenolic substrates: catalysts activity. *J. Hazard. Mater.* **2009**, *162* (2), 588−606.
(58) Miyamoto, S.; Martinez, G. R.; Medeiros, M. H.; Di Mascio, P. Singlet molecular oxygen generated from lipid hydroperoxides by the Russell mechanism: studies using ^{18}O-labeled linoleic acid hydroperoxide and monomol light emission measurements. *J. Am. Chem. Soc.* **2003**, *125* (20), 6172−6179.
(59) Yee, L.; Craven, J.; Loza, C.; Schilling, K.; Ng, N.; Canagaratna, M.; Ziemann, P.; Flagan, R.; Seinfeld, J. Effect of chemical structure on secondary organic aerosol formation from C12 alkanes. *Atmos. Chem. Phys.* **2013**, *13* (21), 11121−11140.
(60) Schilling Fahnestock, K. A.; Yee, L. D.; Loza, C. L.; Coggon, M. M.; Schwantes, R.; Zhang, X.; Dalleska, N. F.; Seinfeld, J. H. Secondary organic aerosol composition from C12 alkanes. *J. Phys. Chem. A* **2015**, *119* (19), 4281−4297.
(61) *Draft screening assessment-certain organic flame retardants substance group: tris (methylphenyl) ester (TCP)*; Health Canada, http://www.ec.gc.ca/ese-ees/default.asp?lang=En&n=B356BCC9-1, 2016.
(62) Lopez-Hilfiker, F. D.; Iyer, S.; Mohr, C.; Lee, B. H.; D'Ambro, E. L.; Kurtén, T.; Thornton, J. A. Constraining the sensitivity of iodide adduct chemical ionization mass spectrometry to multifunctional organic molecules using the collision limit and thermodynamic stability of iodide ion adducts. *Atmos. Meas. Tech.* **2016**, *9* (4), 1505−1512.
(63) Liu, Q.; Liggio, J.; Breznan, D.; Thomson, E. M.; Kumarathasan, P.; Vincent, R.; Li, K.; Li, S. M. Oxidative and toxicological evolution of engineered nanoparticles with atmospherically relevant coatings. *Environ. Sci. Technol.* **2019**, *53* (6), 3058−3066.
(64) Liagkouridis, I.; Cousins, A. P.; Cousins, I. T. Physical−chemical properties and evaluative fate modelling of 'emerging' and 'novel' brominated and organophosphorus flame retardants in the indoor and outdoor environment. *Sci. Total Environ.* **2015**, *524*, 416−426.
(65) Prinn, R.; Huang, J.; Weiss, R.; Cunnold, D.; Fraser, P.; Simmonds, P.; McCulloch, A.; Harth, C.; Salameh, P.; O'doherty, S.; Wang, R. H. J.; Porter, L.; Miller, B. R. Evidence for substantial

DOI: 10.1021/acs.est.9b05327
Environ. Sci. Technol. 2019, 53, 14398−14408

variations of atmospheric hydroxyl radicals in the past two decades. *Science* **2001**, *292* (5523), 1882−1888.
(66) Lawrence, M. G.; Jockel, P.; von Kuhlmann, R. What does the global mean OH concentration tell us? *Atmos. Chem. Phys.* **2001**, *1* (1), 37−49.
(67) Li, C.; Wei, G.; Chen, J.; Zhao, Y.; Zhang, Y. N.; Su, L.; Qin, W. Aqueous OH radical reaction rate constants for organophosphorus flame retardants and plasticizers: experimental and modeling studies. *Environ. Sci. Technol.* **2018**, *52* (5), 2790−2799.

DOI: 10.1021/acs.est.9b05327
Environ. Sci. Technol. 2019, 53, 14398−14408